J Therm Anal Calorim (2014) 115:1525–1531
DOI 10.1007/s10973-013-3470-z

Morphology and thermal characterization of montmorillonite/polybenzimidazole nanocomposite

Bilge Eren · Reyhan Aydin · Erdal Eren

Received: 18 March 2013 / Accepted: 9 October 2013 / Published online: 7 November 2013

Abstract In this study, thermal and morphological properties of organically modified montmorillonite (mMMT)/poly(2,5-benzimidazole) (ABPBI) composite were investigated. The morphology and structure of mMMT/ABPBI composites were characterized by infrared, X-ray diffraction, scanning electron microscopy, and thermogravimetric analysis techniques. At low mMMT loading levels, exfoliation was the predominant mechanism of mMMT dispersion. At high mMMT loading levels, nonintercalated microcomposite morphology is partially favored in expense of the intercalated nanocomposite. Thermal degradation of nanocomposite occured in three stages. In the second stage of thermal degradation, the onset temperature of degradation for the mMMT/ABPBI nanocomposites was lower than that of ABPBI polymer. In the last stage, the improvement in thermal stability by the introduction of mMMT into the ABPBI was different from the second stage. The activation energy for degradation of ABPBI increased from 62.6 to 77.7 kJ mol^{-1} after loading of 5 mass% of mMMT into ABPBI matrix under air atmosphere.

Keywords Proton conductive · Membrane · Polybenzimidazole · Thermal oxidation · Kissinger method

Introduction

Proton exchange membranes (PEMs) are the most important part in PEM fuel cells (PEMFCs). Nafion® is the most widely accepted and commercialized membrane and possesses excellent electro–chemical properties below 80 °C under highly humidified conditions. But, it was reported a decrease in the proton conductivity of Nafion® above 80 °C and under lower humidity conditions [1]. In order to solve this problem, new materials were studied in recent years such as nanocomposites [2, 3], acid loaded polybenzimidazole (PBI) [4–6], and fluorinated and aromatic hydrocarbon membranes [7]. In these materials, PBI and its organic and inorganic composites were the mostly studied materials due to their attractive properties of high thermal stability, excellent mechanical property, low gas permeability, zero water electro-osmotic drag, and high CO tolerance [4–6].

In recent years, polymer/clay nanocomposites have received great interest due to the enhanced properties, such as mechanical [8], thermal [9–11], and barrier properties [12], compared to conventional micron size fillers. These enhanced properties result from combination of organic polymers and only a 2–5 % addition of the nanostructure. Insertion of polymer chains in the MMT layer is a successful approach to synthesize nanocomposite materials [13, 14]. Since the polymer matrix is relatively incompatible with the MMT phase, organic treatment of the layered MMT is required for compatibility with the polymer. The surface modification of MMT from hydrophilic to organophilic is achieved by ion exchange between the hydrated interlayer cations of MMT and cationic surfactants. This process also causes an increase in interlayer space. Polymer chains are more compatible with the modified MMT and able to intercalate within the MMT galleries. Due to the size of the polymer molecules, the interlayer distance of MMT increases to such an extent that exfoliated silicate layers in nanometer dimension might appear.

Poly(2,5-benzimidazole) is an alternative benzimidazole type polymer with thermal stability and conducting

B. Eren (✉) · R. Aydin · E. Eren
Department of Chemistry, Faculty of Science and Arts, Bilecik Seyh Edebali University, 11210 Bilecik, Turkey
e-mail: bilge.eren@bilecik.edu.tr

properties as good as those of PBI. Furthermore, ABPBI with very high molecular masses can be synthesized via simpler and cheaper methods than with PBI [15, 16]. One of the most promising composite systems for use as PEMs is ABPBI nanocomposites [13–18]. Therefore, this study is aimed to establish possible correlations between morphological and thermal degradation properties in the MMT/ABPBI nanocomposite prepared by solution intercalation. In order to better understand the chemical transformations and decomposition process of this polymer nanocomposite during thermal oxidation, scanning electron microscopy (SEM), X-ray diffraction (XRD), Infrared (IR), and isoconversional kinetic analysis have been used to observe the structural changes and the activation energy during thermooxidative degradation.

Experimental

Polymer synthesis

Poly(2,5-benzimidazole) (ABPBI) was prepared by condensation of 3,4-diaminobenzoic acid (DABA) monomers in polyphosphoric acid (PPA). The polymerization was carried out heating a solution of 3.040 g (20 mmol) of DABA in 50 g of PPA (85 % P_2O_5) at 200 °C for 5 h under nitrogen. The polymer was isolated by precipitation in water, filtered, and washed repeatedly with water. To eliminate residual phosphoric acid, the polymer was washed with 10 % NaOH stirring overnight. The dark purple polymer became brown after the NaOH addition. NaOH was eliminated by washing with water to neutrality and boiling the polymer in water for 6 h, three times. The purified polymer was dried at 100 °C for 24 h and 200 °C for another 24 h. A brown fibrous polymer was obtained.

Synthesis of organically modified montmorillonite

To make an organically modified montmorillonite (mMMT) for better dispersion in ABPBI matrix, 2 g of MMT was completely suspended in 100 mL of deionized water at 80 °C with vigorous stirring for 4 h. The aqueous solution of hexadecyltrimethylammonium (HDTMA) was prepared separately by dissolving HDTMA (1.5 times the cation exchange capacity of clay) in 50 mL of distilled water at 80 °C. Then, this solution was added to the dissolved MMT solution and mixed for a further 6 h at 80 °C. The mMMT was washed repeatedly with fresh hot deionized water until no further AgCl formed with titration with 0.1 N $AgNO_3$. The product was then filtered and dried in a vacuum oven at 80 °C for 24 h. The dried cake was ground and screened with a 325-mesh sieve to obtain the mMMT.

Preparation of the mMMT/ABPBI nanocomposite

The nanocomposites were prepared by mixing the appropriate amounts of the ABPBI with 5, 10, 15, and 20 mass% of mMMT in DMAc as a solvent in a flask for a particular concentration. The solution was agitated to high-speed stirring at 80 °C for 2 h and then at 40 °C for 20 h. Thin nanocomposite was obtained by pouring the hybrid solutions into petri dish. These films were further dried at 80 °C under reduced pressure to a constant mass. These composites were called as 5 % mMMT/ABPBI, 10 % mMMT/ABPBI, 15 % mMMT/ABPBI, and 20 % mMMT/ABPBI, respectively.

Characterization techniques

IR spectra of the samples were recorded in the region from 4,000 to 450 cm^{-1} on a Spectrum-100 FTIR spectrometer. Thermogravimetric (TG) curves and differential thermogravimetric (DTG) curves were recorded at five heating rates (5, 10, 20, 30, and 40 °C min^{-1}) from 30 to 1,000 °C under air atmosphere using a PRIS Diamond TG/DTG apparatus. Samples of exactly 10 mg were put in open alumina crucibles. Typically, three replicates were run for each sample, and the average was reported. Surface morphology was studied using a ZEISS Ultraplus model field emission SEM. The XRD analysis data from the samples were collected using a Rigaku, Miniflex ZD13113 (Japan) diffractometer with Cu Kα radiation (Ni filter).

Results and discussion

Material characterization

XRD analysis is a suitable technique in order to probe nanocomposite morphology by monitoring the position, shape, and intensity of the basal reflection diffraction peaks. In an intercalated nanocomposite structure, the intercalation of the polymer chains usually leads a shift of the diffraction peak toward lower angle values. In an exfoliated nanocomposite structure, diffraction peaks of the silicate layers disappear from the XRD patterns. In a microcomposite structure, the interlayer basal spacings of the silicate stay at same position.

The results of XRD studies for the studied samples were shown in Fig. 1, To identify the structure of the prepared composite, its XRD spectrum was compared with spectra of the raw MMT, and ABPBI as a reference. For the XRD pattern of MMT, one reflection was observed in the region $2° < 2\theta < 8°$ (Fig. 1a). This corresponds to the 5.76 (2θ) value from which the interlamellar distance was found to

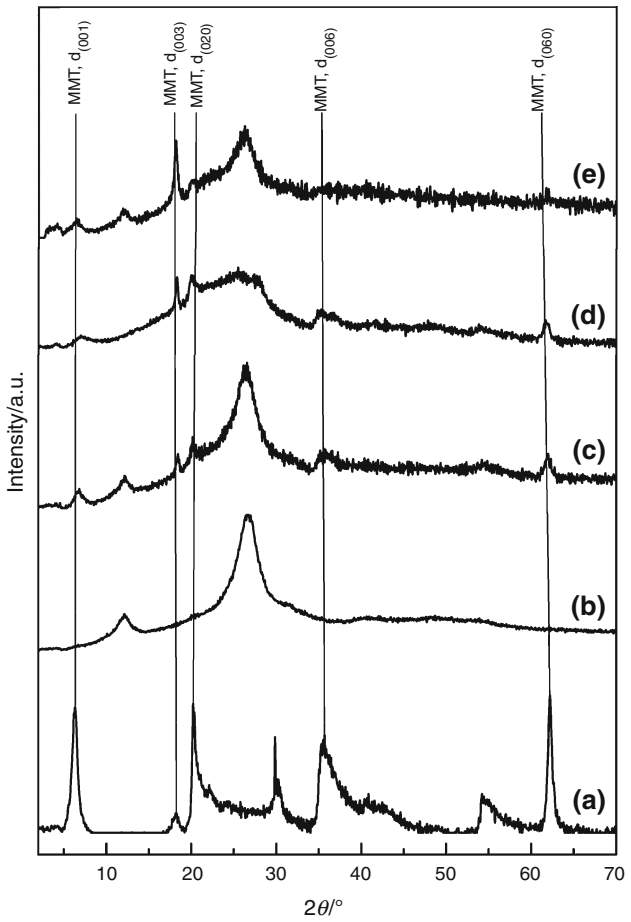

Fig. 1 The XRD patterns of the MMT (*a*), ABPBI (*b*), 5 % mMMT/ABPBI (*c*), 10 % mMMT/ABPBI (*d*), 15 % mMMT/ABPBI (*e*), and 20 % mMMT/ABPBI (*f*)

be 15.33 Å. XRD analysis of ABPBI indicated that it was amorphous in nature (Fig. 1b). ABPBI exhibited two amorphous peaks, indicating that there was two different types of predominant chain packing [19, 20]. A peak corresponding to the lower d-spacing (d_{sp}) of 3.40 Å was dominated by H-bonded region, while other peak at higher d_{sp} of 4.69 Å indicated looser chain packing dominated by bulky substitution. ABPBI has much lower d_{sp} than that of common polymers like polysulfone [21], polyethersulfone [22], etc. This behavior was attributed to the presence of H-bonding in ABPBI that brings chains closer, resulting in efficient chain packing. The characteristic diffraction peak ($2\theta = 5.76°$) disappeared after loading of 5 mass% mMMT into ABPBI matrix (Fig. 1c). This indicated the disordered intercalated or exfoliated structures in mMMT/ABPBI composite [23]. Sample containing 10 mass% of mMMT displayed a small and broad new peak at around 4.86° (Fig. 1d). This new peak became broader, and its intensity increased with increasing mMMT content (Fig. 1e). This result implied that the increase of the loaded mMMT hindered complete exfoliation, and the degree of intercalation increased. The broadening of this peak was also the result of superposition of reflections corresponding to various interlayer distances. At high mMMT contents, the large peak at $2\theta = 5.21°$ in the mMMT/ABPBI material corresponded to the first order (001) reflection of the raw MMT. It showed the undispersed mMMT without ABPBI in the galleries during loading process caused loosening of the intercalated surfactant [24, 25].

SEM images of ABPBI demonstrated that the ABPBI is characterized by an interconnected and highly porous structure (Fig. 2a). SEM image of mMMT/ABPBI composite revealed the presence of irregularly shaped and flaky-like particles, and these flake sheets became much looser and more separated with respect to mMMT (Fig. 2c–f). It was observed that mMMT particles were uniformly distributed in the matrix structure of ABPBI. The fractured surface indicated the high miscibility of the mMMT particles with the matrix and adhesion with the ABPBI. The large cavities on the surface suggested a deficient bonding between the nondispersed mMMT particles and the ABPBI. Furthermore, the dimension of mMMT became smaller compared with the initial particle size suggested the disordered intercalated structure in mMMT/ABPBI nanocomposite Fig. 3.

ABPBI exhibited characteristic absorption bands at 3,399 cm^{-1} and 1,623–1,548 cm^{-1} due to the stretching vibrations of the N–H groups and C=N groups. The presence of a benzimidazole group was confirmed by the characteristic bands at 1,431 cm^{-1}, due to the inplane deformation of the benzimidazole rings. The band at 1,283 cm^{-1} was assigned to the breathing mode of the imidazole ring in ABPBI. In the IR spectrum of the mMMT/ABPBI, the absorption band at 3,627 cm^{-1} was due to OH stretching of Al–OH and Si–OH. Band at 2,922 cm^{-1} was attributed to stretching vibration of C–H aliphatic groups in HDTMA. The characteristic peak 1,035 cm^{-1} was due to the Si–O stretching. The bands in the 400–600 cm^{-1} region that were attributed to Si–O and Al–O bending vibration [26]. The band at 3,417 cm^{-1} was attributed to the isolated N–H stretching of the imidazole. Two absorption bands at 1,625 and 1,574 cm^{-1} confirmed the presence of N–H deformation.

Thermal degradation behavior of MMT/ABPBI composite

The thermal properties of neat ABPBI and ABPBI containing 5, 10, 15, and 20 mass% of mMMT samples were investigated by using DTG in static air atmosphere at a heating rate of 10 °C min^{-1} (Fig. 4). It was observed that the degradation of ABPBI occured in two stages, which was consistent with the results obtained by other researchers for ABPBI [27–30]. The first stage detected

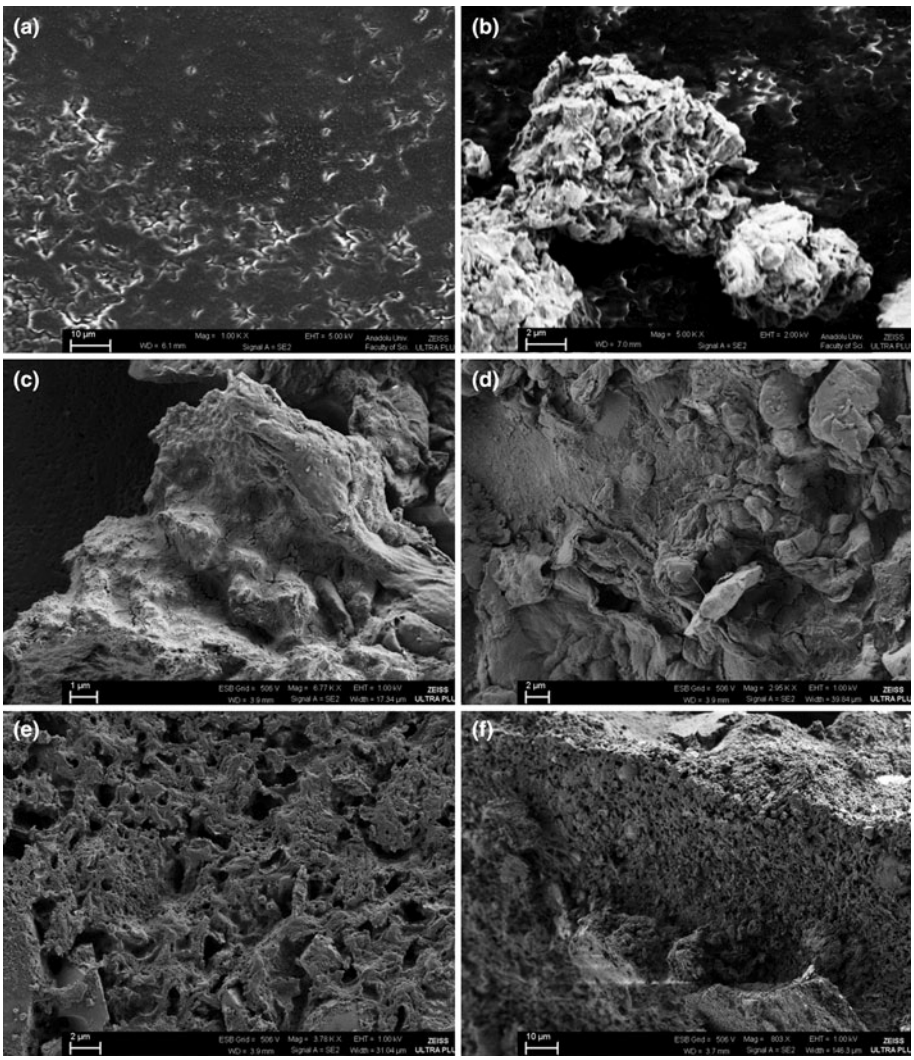

Fig. 2 SEM images of ABPBI (**a**), mMMT (**b**), and an intercalated nanocomposite at different magnifications (**c**–**f**). The mMMT content was 10 %

below 195 °C was linked to the liberation of absorbed water, while the other between 461 and 666 °C referred to the evolution of organic substances. The first step of mass loss for the mMMT/ABPBI nanocomposites occured at about 60–300 °C due to the evaporation of physically absorbed water in the intercalated layers, the loss of hydroxide on montmorillonite layers, and the thermal decomposition of HDTMA alkyl chains [31]. The second step of mass loss takes place at the temperature range of 300–700 °C due to the thermal decomposition of ABPBI chains and formation of charred residues. The T_{onset} of ABPBI was 465 °C and unexpectedly declined to 400, 407, 412, and 431 °C as the loading increased to 5, 10, 15, and 20 mass% of mMMT content, respectively. It was concluded that the HDTMA started to decompose according to the Hofmann elimination reaction or a nucleophilic attack of the ammonium counter-ion on the ammonium [32]. The decomposition products, amines, or acidic protons, enhanced the random chain scission reaction of ABPBI. Also, this result can be attributed that the interlayer cations, such as Mg and/or Al ions, facilitated the thermal degradation of ABPBI. The temperature at the maximum decomposition rate, T_{max}, of neat ABPBI and mMMT/ABPBI nanocomposites containing 5, 10, 15, and 20 % mass of mMMT was determined as 567, 571, 549, 603, and 598 °C, respectively. The yield of charred residue at 900 °C for the mMMT/ABPBI nanocomposites was enhanced from 1.5 % for the neat ABPBI to 5.60 % (charred residue for the mMMT at 900 °C was subtracted). The residue increase was showed that the MMT layers acted as a superior insulator and mass-transport barrier and subsequently reduced the escape of volatile products generated during the thermal decomposition.

The thermo-oxidative degradation activation energy of neat ABPBI and nanocomposites (exfoliated and intercalated samples) containing 5 and 10 mass% of mMMT was calculated by Kissinger method [33] according to the TG data, which were measured under air at different heating rates: 5, 10, 20, 30, and 40 °C min^{-1}. The activation energy for ABPBI and mMMT/ABPBI composites was calculated

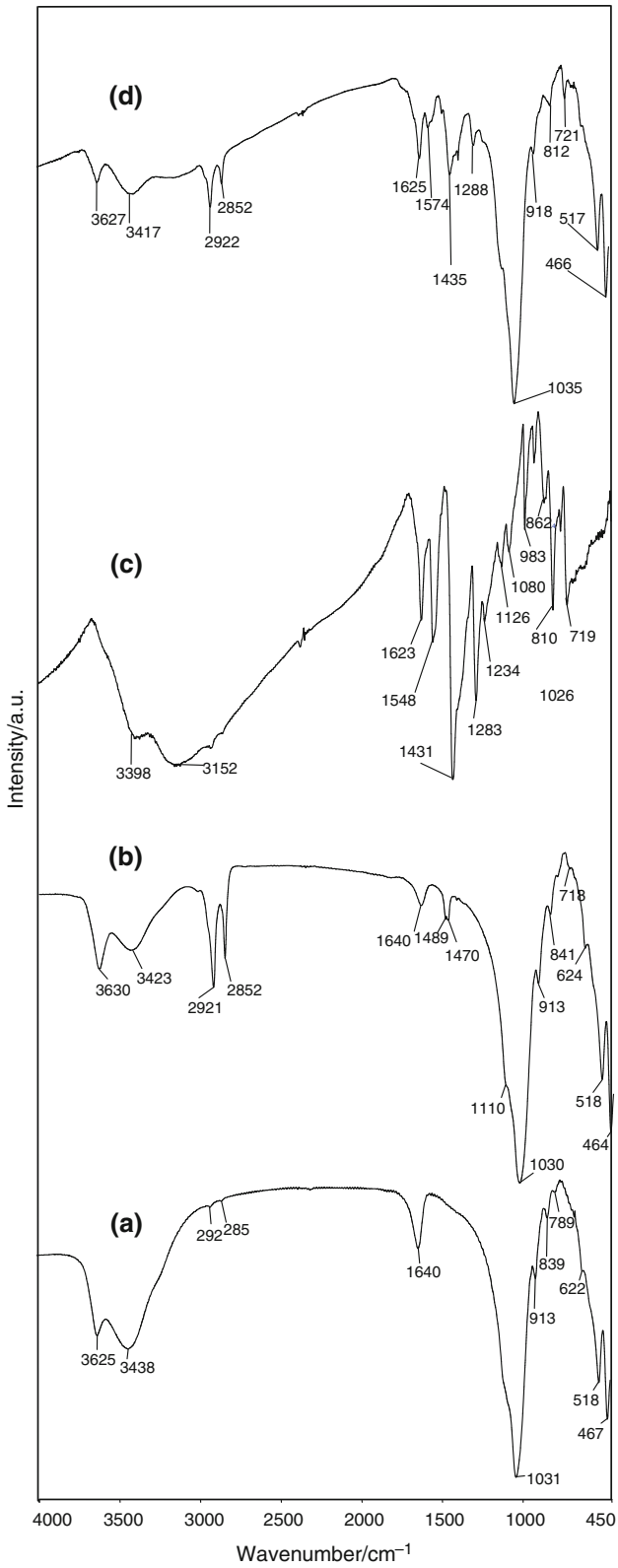

Fig. 3 FTIR spectra for (*a*) MMT, (*b*) mMMT, (*c*) neat ABPBI, and (*d*) an intercalated nanocomposite. The mMMT content was 10 %

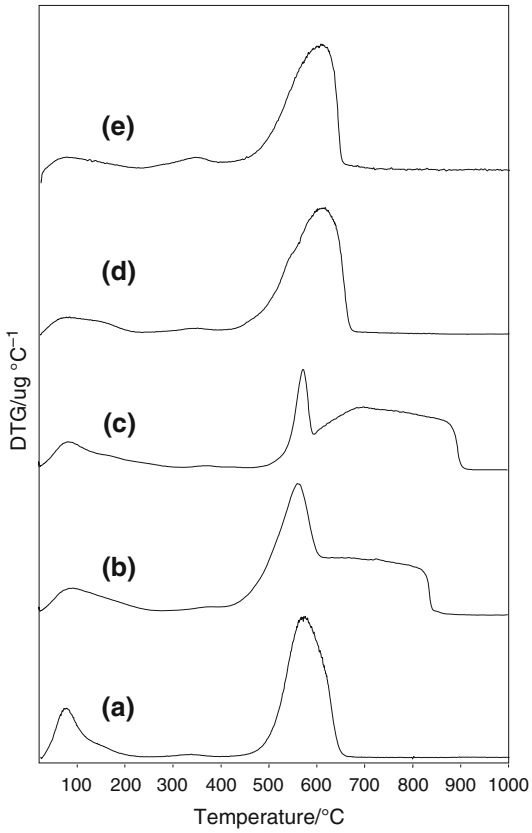

Fig. 4 DTG curves of neat ABPBI (*a*), 5 %—mMMT/ABPBI (*b*), 10 %—mMMT/ABPBI (*c*), 15 %—mMMT/ABPBI (*d*), and 20 %—mMMT/ABPBI (*e*)

from the linear dependence of the $\ln\left(\beta/T_{\max}^2\right)$ versus $1/T_{\max}$ plot (not shown) for various heating rates according to Eq. (1).

$$\ln\left(\frac{\beta}{T_{\max}^2}\right) = \ln\frac{AR}{E_a} - \frac{E_a}{RT_{\max}} \tag{1}$$

In the above equation, A is the preexponential factor, E_a is the apparent activation energy of the degradation reaction, R is the universal gas constant, and β is the heating rate. The activation energy was calculated from the $T_{\max}$, the temperature at which the maximum degradation occurs for different heating rates by assuming that mass loss percentage at $T_{\max}$ is constant. E_a values calculated according to this equation were listed in Table 1. The E_a for degradation of ABPBI found to be 62.6 kJ mol^{-1} under air atmosphere. These values were compatible with the reported literature values [15, 28]. The E_a of ABPBI increased to 77.7 and 287.4 kJ mol^{-1} after loading of 5 and 10 mass% mMMT content into ABPBI matrix under air atmosphere.

Table 1 T_{max} and activation energy values of ABPBI and mMMT/ABPBI samples

mMMT content/mass%		β/°C min^{-1}					E_a/kJ mol^{-1}	R^2
		5	10	20	30	40		
–	T_{max}/°C	567	620	680	720	736	62.6	0.995
5	T_{max}/°C	455	471	522	540	556	77.7	0.936
10	T_{max}/°C	549	561	572	576	592	287.7	0.955

Conclusions

To identify the structures of the prepared nanocomposites, their XRD spectra were compared with that of the raw MMT and ABPBI. In the XRD patterns of nanocomposites, the basal peak of MMT became broader and shifted to lower 2θ values loosing its intensity with increasing the amount of MMT. This result indicated the formation of a nanocomposite structure with the intercalation of ABPBI chains in the gallery of the MMT silicate layers. XRD spectra of nanocomposites showed that the MMT layers lost their parallel stacking, and became partially disordered due to ABPBI entered the MMT layers at low MMT contents. At low mMMT loading, exfoliation was the predominant mechanism of MMT dispersion. The dispersion of mMMT within the ABPBI matrix deteriorated at high mMMT contents. At high mMMT loading, nonintercalated microcomposite morphology is partially favored in expense of the intercalated nanocomposite. The SEM micrograph of the nanocomposite depicted a flaky morphology as opposed to a granular one, suggesting that the ABPBI is, in fact, intercalated into the MMT layers. As shown by SEM, the undispersed particles showed the mMMT agglomeration on the surfaces of ABPBI particles during loading process. Thermal degradation of nanocomposite occured in three stages with various mass percent losses. In the second stage of thermal degradation, the onset temperature of degradation for the mMMT/ABPBI nanocomposites was lower than that of ABPBI polymer. This results showed that the HDTMA used as organophilic modifier enhanced the ABPBI degradation. The onset and end-point temperatures of the second stage TG curve for the nanocomposites were decreased by about 15–20 °C. In the last stage, the improvement in thermal stability by the introduction of mMMT into the ABPBI was different, in the temperature range of 800–1,000 °C. The MMT content of the composites was directly relative to the mass of the residue obtained at 900 °C. The yield of charred residue at 900 °C for the neat ABPBI, 5, 10, 15, and 25 %-mMMT/ABPBI nanocomposites were 1.5, 6.6, 16, 17.3, and 31.6 %, respectively. The enhanced thermal stability of the ABPBI hybrid nanocomposites was attributed to the lower permeability of oxygen and the diffusibility of the degradation products from the bulk of the polymer caused by the exfoliated MMT in the composites.

References

1. Chuang S-W, Hsu SL-C, Liu Y-H. Synthesis and properties of fluorine-containing polybenzimidazole/silica nanocomposite membranes for proton exchange membrane fuel cells. J Membr Sci. 2007;305:353–63.
2. Hasani-Sadrabadi MM, Dashtimoghadam E, Majedi FS, Kabiri K, Solati-Hashjin M, Moaddel H. Novel nanocomposite proton exchange membranes based on Nafion® and AMPS-modified montmorillonite for fuel cell applications. J Membr Sci. 2010;365:286–93.
3. Namazi H, Ahmadi H. Improving the proton conductivity and water uptake of polybenzimidazole-based proton exchange nanocomposite membranes with TiO_2 and SiO_2 nanoparticles chemically modified surfaces. J Power Sour. 2011;196:2573–83.
4. Wang S, Zhao C, Ma W, Zhang G, Liu Z, Ni J, Li M, Zhang N, Na H. Preparation and properties of epoxy-cross-linked porous polybenzimidazole for high temperature proton exchange membrane fuel cells. J Membr Sci. 2012;411–412:54–63.
5. Zhao C, Lin H, Han M, Na H. Covalently cross-linked proton exchange membranes based on sulfonated poly(arylene ether ketone) and polybenzimidazole oligomer. J Membr Sci. 2010;353:10–6.
6. Bai H, Ho WS. New sulfonated polybenzimidazole (SPBI) copolymer-based proton-exchange membranes for fuel cells. J Taiwan Inst Chem E. 2009;40:260–7.
7. Kim DS, Robertson GP, Guiver MD, Lee YM. Synthesis of highly fluorinated poly(arylene ether)s copolymers for proton exchange membrane materials. J Membr Sci. 2006;281:111–20.
8. Chrissafis K, Pavlidou E, Paraskevopoulos KM, Beslikas T, Nianias N, Bikiaris D. Enhancing mechanical and thermal properties of PLLA ligaments with fumed silica nanoparticles and montmorillonite. J Therm Anal Calorim. 2011;105:313–23.
9. Nistor MT, Vasile C. Influence of the nanoparticle type on the thermal decomposition of the green starch/poly(vinyl alcohol)/montmorillonite nanocomposites. J Therm Anal Calorim. 2013;111:1903–19.
10. Cheng HKF, Sahoo NG, Lu XH, Li L. Thermal kinetics of montmorillonite nanoclay/maleic anhydride-modified polypropylene nanocomposites. J Therm Anal Calorim. 2012;109:17–25.
11. Hristodor CM, Vrinceanu N, Pode R, Copcia VE, Botezatu E, Popovici E. Preparation and thermal stability of Al_2O_3-clay and Fe_2O_3-clay nanocomposites, with potential application as remediation of radioactive effluents. J Therm Anal Calorim. 2013;111:1227–34.
12. Malucelli G, Alongi J, Gioffredi E, Lazzari M. Thermal, rheological, and barrier properties of waterborne acrylic nanocomposite coatings based on boehmite or organo-modified montmorillonite. J Therm Anal Calorim. 2013;111:1303–10.
13. Kong QH, Hu Y, Song L, Tang YW. Kinetics of thermo-oxidative degradation of polypropylene/aluminum trihydroxide/organo Fe-montmorillonite nanocomposites. J Therm Anal Calorim. 2011;104:1145–51.
14. Pagacz J, Pielichowski K. PVC/MMT nanocomposites DSC with stochastic temperature modulation study at glass transition region. J Therm Anal Calorim. 2013;111:1571–5.

15. Asensio JA, Borrós S, Gómez-Romero P. Proton-conducting membranes based on poly(2,5-benzimidazole) (ABPBI) and phosphoric acid prepared by direct acid casting. J Membr Sci. 2004;241:89–93.
16. Zheng H, Mathe M. Enhanced conductivity and stability of composite membranes based on poly (2,5-benzimidazole) and zirconium oxide nanoparticles for fuel cells. J Power Sour. 2011;196:894–8.
17. Linlin M, Mishra AK, Kim NH, Lee J. H Poly(2,5-benzimidazole)–silica nanocomposite membranes for high temperature proton exchange membrane fuel cell. J Membr Sci. 2012; 411–412:91–8.
18. Diaz LA, Abuin GC, Corti HR. Methanol sorption and permeability in Nafion and acid-doped PBI and ABPBI membranes. J Membr Sci. 2012;411–412:35–44.
19. Kumbharkar SC, Islam MN, Potrekar RA, Kharul UK. Variation in acid moiety of polybenzimidazoles: ınvestigation of physicochemical properties towards their applicability as proton exchange and gas separation membrane materials. Polymer. 2009;50:1403–13.
20. Kumbharkar SC, Kharu UK. New N-substituted ABPBI: synthesis and evaluation of gas permeation properties. J Membr Sci. 2010;360:418–25.
21. Dai Y, Guiver MD, Robertson GP, Kang YS, Lee KJ, Jho JY. Preparation and characterization of polysulfones containing both hexafluoroisopropylidene and trimethylsilyl groups as gas separation membrane materials. Macromolecules. 2004;37:1403–10.
22. Khayet M, Garcia-Payo MC. X-ray diffraction study of polyethersulfone polymer, flat-sheet and hollow fibers prepared from the same under different gas-gaps. Desalination. 2009;246:121–7.
23. Raka L, Bogoeva-Gaceva G, Loos J. Characterization of polypropylene/layered silicate nanocomposites prepared by single-step method. J Therm Anal Calorim. 2010;100:629–39.
24. Park Y, Ayoko GA, Kristof J, Horvath E, Frost RL. Thermal stability of organoclays with mono- and di-alkyl cationic surfactants. J Therm Anal Calorim. 2012;110:1087–93.
25. Elkhalifah AEI, Maitra S, Bustam M, Murugesan T. Thermogravimetric analysis of different molar mass ammonium cations intercalated different cationic forms of montmorillonite. J Therm Anal Calorim. 2012;110:765–71.
26. Lalikova S, Pajtasova M, Chromcikova M, Liska M, Sutinska V, Olsovsky M, Ondrusova D, Mojumdar SC. Investigation of natural rubber composites with addition of montmorillonite fillers using thermal analysis. J Therm Anal Calorim. 2011;104:969–73.
27. Asensio JA, Borrós S, Gómez-Romero P. Sulfonated poly(2,5-benzimidazole) (SABPBI) impregnated with phosphoric acid as proton conducting membranes for polymer electrolyte fuel cells. Electrochim Acta. 2004;49:4461–6.
28. Asensio JA, Borrós S, Gómez-Romero P. Proton-conducting polymers based on benzimidazoles and sulfonated benzimidazoles. J Polym Sci Part A. 2002;40:3703–10.
29. Zhenga H, Petrik L. Mathe M Preparation and characterisation of porous poly(2,5benzimidazole) (ABPBI) membranes using surfactants as templates for polymer electrolyte membrane fuel cells. Int.J Hydrogen Energ. 2010;35:3745–50.
30. Zheng H, Luo H, Mathe M. Proton exchange membranes based on poly(2,5-benzimidazole) and sulfonated poly(ether ether ketone) for fuel cells. J Power Sour. 2012;208:176–9.
31. Dweck J, Barreto EP, Meth S, Buchler PM. Partially exchanged organophilic bentonites. J Therm Anal Calorim. 2011;105:907–13.
32. Zhao C, Qin H, Gong F, Feng M, Zhang S, Yang M. Mechanical, thermal and flammability properties of polyethylene/clay nanocomposites. Polym Degrad Stab. 2005;87:183–9.
33. Kissinger HE. Anal Chem. 1957;11:1702–6.